

Investigation of HDD Ramp Unloading Processes with an Efficient Scheme

Yan Liu and Hejun Du*

*School of Mechanical and Aerospace Engineering, Nanyang Technological
University, 50 Nanyang Avenue, Singapore 639798, Singapore*

Received 30 December 2009; Accepted (in revised version) 17 May 2011

Available online 31 October 2011

Abstract. Ramp load/unload (L/UL) mechanisms are widely used to rest sliders in hard disk drives (HDDs). Loading/unloading a slider swiftly and smoothly is crucial in a HDD design. A novel, efficient simulation scheme is proposed to investigate the behaviors of a head disk interface (HDI) in ramp unloading processes. A dual scale model is enabled by decoupling the nano-meter scale change of an air bearing and the micro- or milli-meter scale deformation of a suspension. A modified Reynolds equation governing the air bearing was solved numerically. The slider design was characterized with performance functions. Three stages in an unloading process were analyzed with a lumped parameter suspension model. Key parameters for the model were estimated with a comprehensive finite element suspension model. Finally, simulation results are presented for a commercial HDI design.

AMS subject classifications: 65P40

Key words: Hard disk drive, ramp, unloading, head-disk interface, suspension, Reynolds equation, performance surfaces.

1 Introduction

Hard disk drives (HDDs) provide a major form for data storage. To address the serious tribological problems caused by the direct contact between the disk and the head, floating sliders are designed to suspend the heads above the disk surfaces as the disks passed by underneath. Nowadays, minimum flying height of a magnetic slider is approaching 5nm and even below. When a HDD is powered off, the rotational speed of the disks slows down to stop, and therefore the dynamic air bearing supporting the slider disappears. To avoid the direct slider-disk contact, the sliders should land on

*Corresponding author.

URL: <http://www.ntu.edu.sg/home/mhdu/>

Email: mhdu@ntu.edu.sg (H. J. Du)

a non-data zone before the air bearing breaks down. Load/unload (L/UL) mechanisms are widely adopted to resist wear and tolerate more start/stop cycle by resting a slider on a ramp [1, 2]. A typical ramp L/UL mechanism is shown in Fig. 1. Currently, L/UL zone at the outer disk diameter is not used for data storage due to potential loss of magnetic information caused by head-disk contact. If the slider can be loaded/unloaded smoothly and swiftly, the L/UL zone can be minimized or even be used for data storage, and then a larger storage area is available.

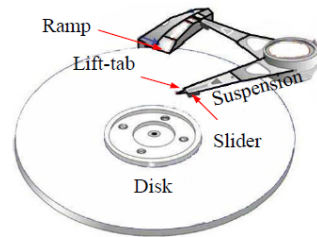


Figure 1: A typical load/unload mechanism in HDD.

Simulation provides an economical approach for a HDI design. In a conventional dynamics analysis, the instantaneous attitude of a slider was calculated by solving a modified Reynolds equation which was coupled through the air bearing force and the moment with the dynamics of the suspension [3–5]. The historical behaviors in an unloading process were obtained by solving the coupled equations repeatedly. Despite its precision, the traditional way is limited to examining only typical, individual cases because of the intensive computation requirements.

In this work, an efficient scheme is proposed to analyze the behaviors of subambient pressure sliders in unloading processes. The studies on the sliders and the suspensions are decoupled with a dual-scale model. The numerical solutions for a modified Reynolds equation were fitted to characterize the performance of an air bearing design. A simplified lumped parameter model was constructed to study the behaviors of a suspension in unloading processes. Key parameters of the suspension were estimated with a comprehensive finite element model and checked with experiments. With the efficient scheme, an unloading simulation can be worked out with a very short computation time [6,7].

2 Analysis of an unloading process

2.1 Three stages in an unloading process

In modern HDDs, a head-gimbal assembly (HGA) is designed with several pieces as shown in Fig. 2(a). The load beam helps position the slider. The gimbal allows the flying slider to rotate about the dimple to accommodate surface variations. The limiter is designed to limit the separation between the load beam and the slider. The lift tab

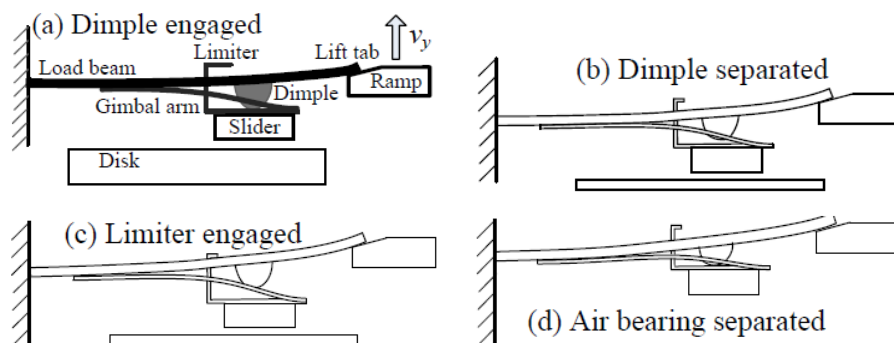


Figure 2: Three stages in unloading processes.

attached to the end of a suspension moves along a ramp located at the outer edge of the disk, enabling the loading and unloading processes of the slider.

In a normal operating condition, the slider is positioned at the nominal minimum flying height. The spring force from the deformed load beam is balanced by the air bearing force generated by a thin air layer squeezed into the narrow space between the slider and the disk surface. Although it provides very low and stable flying heights, the subambient pressure design negatively affects the performance of the sliders and the suspensions during the L/UL processes [8].

A HGA may experience three stages in an unloading process as shown in Figs. 2(a)-(d), namely the dimple engaged, the dimple separated, and the limiter engaged [9,10]. In the stage of dimple engaged, the dimple and gimbal take effect together. As the ramp being raised up, the dimple separates from the slider and the gimbal takes effect alone. When the gap between the slider and the suspension is stretched too much, the limiter engages with the suspension. Thereafter, the limiter and the gimbal take effect together till the air bearing breaks up. The slider separates from the disk. The suspension exhibits different mechanical properties in each stage due to the different combination of the components. An unloading time is defined as the time elapsed between the instant when the lift-tab touches the ramp and the instant when the slider separates from the disk. The unloading distance is defined as the lateral span that the slider runs during the unloading time. The unloading status and the unloading distance are shown in Fig. 3.

2.2 Air bearing constraint forces and transitional conditions for stages

A local lumped parameter model shown in Fig. 4 was constructed to study the conditions for the stage transition.

In dimple engaged stage, the dimple and the gimbal together take effect to balance the air bearing force. The air bearing force during the stage can be solved with Eq. (2.1)

$$F_s = k_d(L_d - L_s) - k_g(L_s - L_g), \quad (2.1)$$

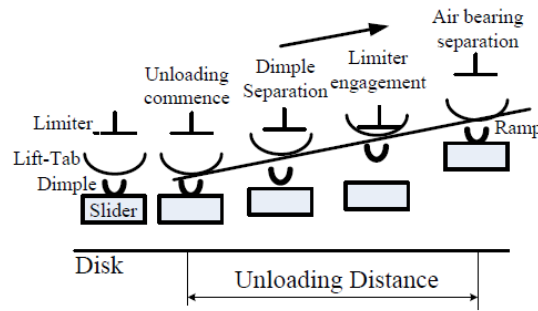


Figure 3: Unloading distance.

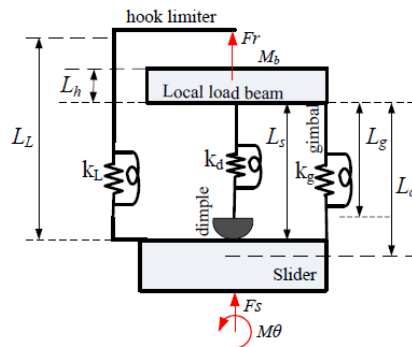


Figure 4: A local lumped parameter suspension model.

where F_s is the air bearing force, k_d and k_g are the stiffnesses of the dimple and the gimbal, respectively, L_s is the gap between the load beam and the slider, L_d and L_g are the free lengths of the dimple and the gimbal, respectively.

After the dimple separates from the slider, only the gimbal takes effect to balance the air bearing force. The air bearing force during the stage can be solved with Eq. (2.2)

$$F_s = -k_g(L_s - L_g). \tag{2.2}$$

After the limiter contacts the load beam, the limiter and the gimbal together take effect to balance the air bearing force. The air bearing force during the stage can be solved with

$$F_s = -k_g(L_s - L_g) - k_L(L_L - L_h), \tag{2.3}$$

where k_L is the stiffnesses of the limiter, L_L is the free lengths of the limiter, L_h is the thickness of the slider.

The air bearing force will degrade from a positive value to a negative value in the dimple engaged stage when $F_s = 0$. The gap L_s at the moment can be worked out with

$$L_s = \frac{k_d L_d + k_g L_g}{k_g + k_d}. \tag{2.4}$$

The dimple separates from the slider when $L_d = L_s$. The air bearing force at the moment can be expressed with

$$F_s = -k_g(L_d - L_g). \quad (2.5)$$

The limiter engages with the load beam when $L_L = L_s + L_h$. The air bearing force at the moment can be expressed with

$$F_s = -k_g(L_L - L_h - L_g) - k_L(L_L - L_h). \quad (2.6)$$

3 Three DOF suspension model and parameter estimation

3.1 A dual scale model for HDI

Compared with the vibration frequency of the slider and the suspension, an unloading duration is long enough to be studied quasi-statically.

The forces and the moment on the key components can be calculated with

$$\begin{Bmatrix} F_s - F_{s0} \\ M_\theta - M_{\theta 0} \\ F_r - F_{r0} \end{Bmatrix} = \begin{bmatrix} k_{ss} & k_{s\theta} & k_{sr} \\ k_{\theta s} & k_{\theta\theta} & k_{\theta r} \\ k_{rs} & k_{r\theta} & k_{rr} \end{bmatrix} \begin{Bmatrix} z_s - z_{s0} \\ \theta - \theta_0 \\ z_r - z_{r0} \end{Bmatrix}, \quad (3.1)$$

where F_s and M_θ are the air bearing constraint force and moment on the slider, respectively, F_r is the vertical force on the lift tab, z_s and θ are the position and the attitude of the slider, respectively, z_r denotes the position of the lift tab, the subscript 0 denote the values of each variable in the normal operating condition, k_{xx} in the matrix denote stiffness coefficients of the suspension.

In an unloading process, the change of the flying height can be 1000 times smaller than the deformation of the suspension. When the suspension is studied, the air bearing effect is represented by displacement constraints while the gap of an air bearing is neglected. Thus, it is assumed that the slider makes completely contact with the disk surface before the instant of air bearing separation as viewed from the suspension. The instantaneous force and moment acting on the slider at this stage can be solely determined from the deformations of the suspension expresses with

$$\begin{cases} F_s = k_{sr}(z_r - z_{r0}) + F_{s0}, \\ M_\theta = k_{\theta r}(z_r - z_{r0}) + M_{\theta 0}. \end{cases} \quad (3.2)$$

3.2 Parameter estimation with FEM

k_{sr} and $k_{\theta r}$ were estimated with a comprehensive finite element model (FEM). In the FEM, solid elements were used to model the actuator arm, the dimple, the limiter and the slider. Shell elements were used to model the hinge, the gimbal and the load beam. Since the dimple may contact with the tongue of the gimbal while the limiter may contact with the top surface of the load beam in an unloading process, contact

pairs were included to model the contact interfaces. The limiter and the dimple were modeled as the target surfaces while the top of the load beam and the back of the gimbal were modeled as contact surfaces.

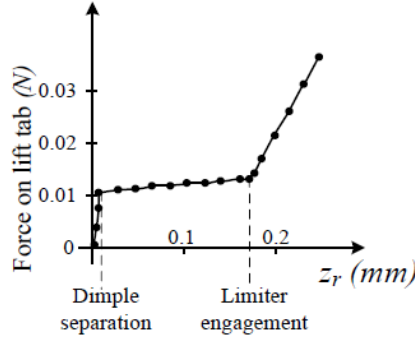


Figure 5: History of the force on the lift tab in the unloading process.

Static structural analyses were performed to determine the changes of the displacements and the forces on the suspension. Nodal imposed (nonzero) displacements were applied on the four corners of the slider and the lift tab. Their corresponding nodal reaction forces were checked. By keeping the slider stationary, namely

$$z_s - z_{s0} = 0 \quad \text{and} \quad \theta - \theta_0 = 0,$$

and changing z_r , k_{sr} and $k_{\theta r}$ can be figured out with Eqs. (3.3a) and (3.3b), respectively. The nodal imposed displacements and the DOF constraint were set up carefully to mimic different states in unloading processes

$$k_{sr} = \frac{\Delta F_s}{\Delta Z_r}, \tag{3.3a}$$

$$k_{\theta r} = \frac{\Delta M_\theta}{\Delta Z_r}, \tag{3.3b}$$

where ΔF_s and ΔM_θ are the changes of the constraint force and moment on the slider, respectively. The values of k_{sr} in dimple engaged, dimple separated, and limiter engaged are $-2470(N/m)$, $-12(N/m)$ and $-480(N/m)$, respectively. The values of $k_{\theta r}$ in dimple engaged, dimple separated, and limiter engaged are $1.67 \times 10^{-2}(N/rad)$, $2.92 \times 10^{-3}(N/rad)$ and $3.83 \times 10^{-1}(N/rad)$, respectively. The history of F_r in the analysis is illustrated in Fig. 5. Graphically, the equivalent free lengths of the gimbal and the limiter from the respective of the lift tab are 0.005mm and 0.175mm, respectively.

4 Air bearing model and performance functions

4.1 Air bearing model and numerical solution

In modern HDDs, a head-disk interface (HDI) is designed as an air bearing. Reynolds equation yields accurate results when K_n is less than 0.001, which corresponds to the

continuum flow regime. The Knudsen number which is the ratio of the mean free path of gas molecules γ to the available range of movement h is used to measure the degree of gas rarefaction at thin film thicknesses ($K_n = \gamma/h$). Nowadays, the air bearing gap goes below ten nanometers and is smaller than the mean free path of the air (about 64nm under standard conditions). The gas in such a small gap loses its continuity and slips against the surface [11]. Thus the HDI is modeled with a modified Reynolds equation below, which cast a similar form to the Reynolds equation [12–16]

$$\frac{\partial}{\partial X} \left(Q_p P H^3 \frac{\partial P}{\partial X} - \Lambda_x P H \right) + \frac{\partial}{\partial Y} \left(Q_p P H^3 \frac{\partial P}{\partial Y} - \Lambda_y P H \right) = \sigma \frac{\partial(PH)}{\partial T}, \quad (4.1)$$

where P and H are the dimensionless pressure and distance between air bearing surface and disk surface, normalized by p_a and h_m , respectively; T equals to ωt , σ denotes the squeeze number.

$$\Lambda_x = (6\mu U_x L) / (p_a h_m^2), \quad \text{and} \quad \Lambda_y = (6\mu U_y L) / (p_a h_m^2)$$

are the bearing numbers in the x and y directions, respectively, $\sigma = (12\mu\omega L^2) / (p_a h_m^2)$ is the squeeze number. U_x and U_y are the disk velocity components in the x and y direction, μ is the dynamic viscosity of the gas, L is the length scale of the slider, Q_p is a Poiseuille flow rate coefficient which reflects the type of slip correction.

Various slip correction models have been proposed. Burgdorfer raised a first-order model by considering slipping and heat conduction. To increase the accuracy of the slip-flow model, Hsia and Domoto derived a second-order modified Reynolds equation using slip-flow boundary conditions for both shear and pressure flows. Mitsuya introduced the 1.5-order slip model in order to predict the load capacity more accurately from the physical considerations that taking account of the accommodation coefficient into account. Gans, who first treated the linearized Boltzmann equation as a basic equation, derived the approximation lubrication equation analytical using a successive approximation method. Fukui and Kaneko started from the linearized Boltzmann equation based on the BGK model and introduced the use of a Poiseuille flow database to allow a quicker computation of a generalized lubrication equation for high K_n number gas bearing [17].

The surface of a subambient slider is typically etched with embossed pads and recessed cavities. Negative (subambient) pressure tends to be generated at the cavity area and the positive (above-ambient) pressure forms at the pad areas in operation. The geometrical (clearance) discontinuities of a slider profiles caused by Walls of the recesses and pads lead numerical difficulty for finite difference methods based on the differential form of the modified Reynolds equation. Finite volume method, instinctively suitable for solving the modified Reynolds equation with discontinued profiles, was adopted [18]. The key step is the integration of the modified Reynolds equation over a two-dimensional control volume.

A typical subambient slider is shown in Fig. 6. Since the load/unload mechanism situates at the out edge of the disk, the point of interest is set on a 1 inch disk at radius

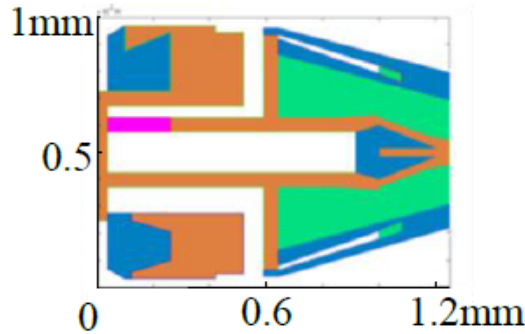


Figure 6: Surface profile of a slider.

of 11.682mm with skew angle of 9.861 degree. The disk rotational speed is 3600rpm. The slider is considered flying with a zero roll angle. The air pressure distribution on the surface of the subambient slider shown in Fig. 7 was solved with the FVM scheme when $h_{\min} = 10\text{nm}$ and $\theta = 80\mu\text{rad}$. The 1.5-order slip model is adopted.

We can observe the subambient pressure at the recess area and above ambient pressure at the pad area. Considering the ambient pressure on both the reverse and obverse sides of the slider, the total air bearing force on the slider is obtained by integrating the pressure over the entire slider area on both sides with Eq. (4.2a). Moments is calculated out with respect to the geometric center of the slider using Eq. (4.2b).

$$F_a = \iint [p(x, y) - 1] dx dy, \tag{4.2a}$$

$$M_a = \iint \left(1 - \frac{x_0}{2}\right) [p(x, y) - 1] dx dy, \tag{4.2b}$$

where $p(x, y)$ is the pressure on the nodes. x_0 is the loading point.

4.2 Performance surfaces for air bearing design

The air bearing force and moment of the slider for an arbitrary attitude are obtained by fixing the pitch angle and the minimal flying height and solving Eq. (4.1). For a

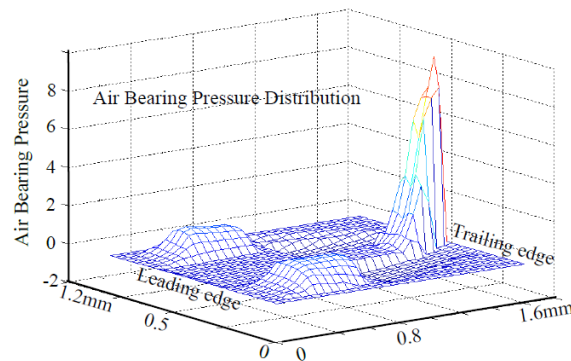


Figure 7: Surface profile of a slider.

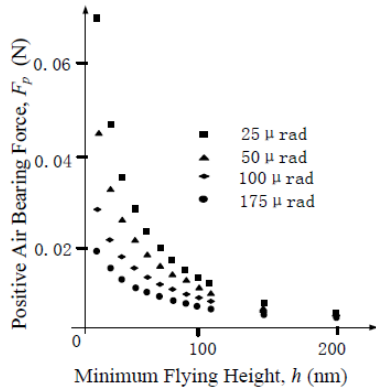


Figure 8: F_p vs h for varying pitch angles.

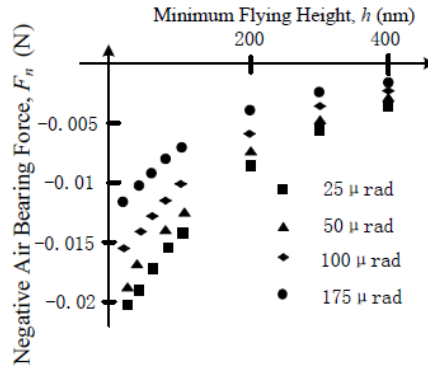


Figure 9: F_n vs h for varying pitch angles.

positive pitch angle, the leading edge spacing is larger than the trailing edge spacing. The positive forces and negative forces for the abovementioned slider with varying attitudes were plotted in Figs. 8 and 9, respectively.

Generally, the discrete points for varying attitudes were fitted with performance functions expressed in Eqs. (4.3) and (4.4), in which the minimum flying height h and the pitch angle θ were chosen as the attitude variables

$$F_a(h, \theta) = F_p(h, \theta) + F_n(h, \theta) = a(\theta) \cdot e^{-b(\theta)h^m} + c(\theta) \cdot e^{-d(\theta)h^n}, \quad (4.3)$$

where F_p , F_n and F_a are the positive force, negative force and total air bearing force, respectively, a , b , c and d are variables for different subambient designs

$$M_a(h, \theta) = M_p(h, \theta) + M_n(h, \theta) = f(\theta) \cdot e^{-u(\theta)h^i} + w(\theta) \cdot e^{-v(\theta)h^j}, \quad (4.4)$$

where M_p , M_n and M_a are the positive moment, negative moment and total moment, respectively, f , u , w and v are variables for different subambient designs.

The performance force functions for the aforementioned subambient pressure slider are expressed with Eqs. (4.5a), (4.5b) and (4.5c) are illustrated with Figs. 10, 11 and 12,

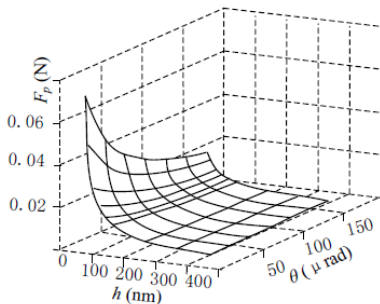


Figure 10: Performance surface of positive air bearing force.

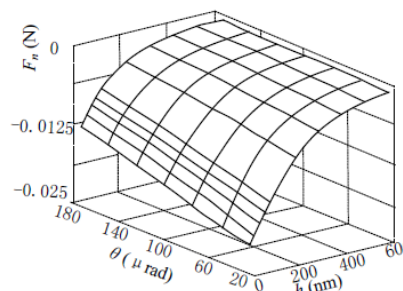


Figure 11: Performance surface of negative air bearing force.

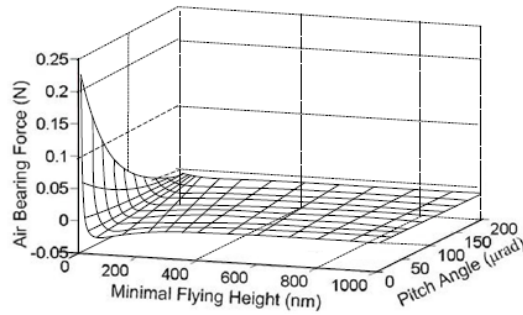


Figure 12: Performance surface of total air bearing force.

respectively

$$F_p(h, \theta) = 0.257e^{-0.015\theta - (5.561 \times 10^{-6}\theta^2 - 0.002\theta + 0.341)h^{0.5}}, \tag{4.5a}$$

$$F_n(h, \theta) = (6.182 \times 10^{-5}\theta - 0.024)e^{-(1.101 \times 10^{-5}\theta + 0.008)h^{0.9}}, \tag{4.5b}$$

$$F_a(h, \theta) = F_p(h, \theta) + F_n(h, \theta). \tag{4.5c}$$

Similarly, the performance moment functions for the slider can be expressed with Eq. (4.6a) to Eq. (4.6c)

$$M_p(h, \theta) = (7.926 \times 10^{-4})e^{-0.019\theta - (4.1 \times 10^{-5}\theta^2 - 0.014\theta + 2.772)h^{0.2}}, \tag{4.6a}$$

$$M_n(h, \theta) = -(2.572 \times 10^{-5})e^{-0.012\theta - (6.4 \times 10^{-7}\theta^2 - 1.8 \times 10^{-4}\theta + 0.021)h}, \tag{4.6b}$$

$$M_a(h, \theta) = M_p(h, \theta) + M_n(h, \theta), \tag{4.6c}$$

where M_p and M_n are the positive and the negative air bearing moment, respectively.

5 Simulation for an unloading process

Since F_s is identical to F_a while M_θ is identical to M_s before the air bearing separation, the instantaneous h and θ can be obtained using the following equations in a very short computational time:

$$\begin{cases} F_a(h, \theta) = F_s, \\ M_a(h, \theta) = M_\theta. \end{cases} \tag{5.1}$$

5.1 Case studies with the efficient scheme

Simulations based on a commercial HDD are performed on a personal computer with a 1.86-GHz Pentium processor and 1GB RAM. The histories of the forces are illustrated in Fig. 13. Notice that three stages are observed with the existing design. The limiter engagement with the load beam helped to raise the slider. Lateral velocity was given as 0.120m/s and the slope of the ramp is 12° . The air bearing force reaches its

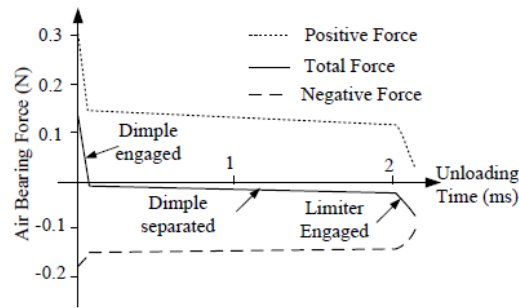


Figure 13: Histories of the air bearing forces in an unloading process.

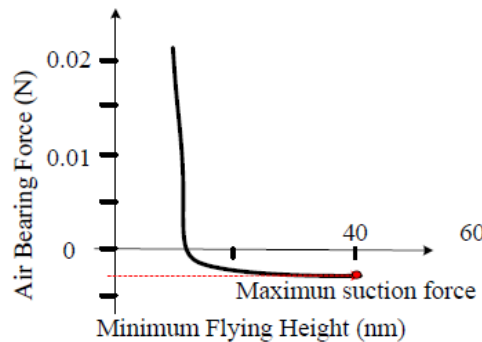


Figure 14: F_a vs h in an unloading process.

maximum suction force (the derivative of the curve equals to zero) when the minimal flying height is 40.67nm as shown in Fig. 14. At the instant, the lift tab is still being raised and there is no bigger air bearing force to hold the slider, the air bearing breaks up. The pitch angle at the moment was $175\mu\text{rad}$. The unloading time was 2.2ms.

The calculation for the unloading process (up to the air bearing separation) took only tens of seconds or no more than one minute depending on the number of the numerical steps and the parameters of the suspension, whereas it takes hours or even days to figure it out using traditional methods.

The scheme is very efficient. As an example, the effects of varying stiffnesses of

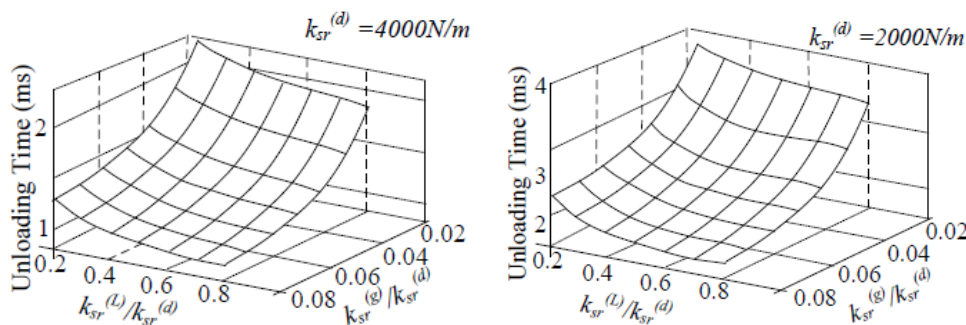


Figure 15: The effects of the stiffnesses on the unloading time.

the suspension on the unloading time are studied and shown in Fig. 15. By changing the ratio of the stiffnesses, the trend of the unloading time can be figured out in tens of minutes, much faster than using traditional schemes for HDI studies. The superscripts (*d*), (*g*) and (*L*) denote the stages before dimple separation, after dimple separation but before limiter engagement, and after limiter engagement, respectively.

6 Conclusions

An efficient simulation scheme for studying the performance of HDIs in unloading processes was developed in the paper.

1. A dual scale model focusing on the slider and the lift tab was constructed to decouple the studies on the air bearings and the suspensions. Three stages and transitional conditions in an unloading process were discussed.
2. A lumped parameter suspension model focusing on key parameters was raised. A comprehensive finite element model was constructed to estimate the values of the parameters.
3. A general procedure for characterizing the subambient pressure slider designs with performance functions and surfaces was presented. The instantaneous attitude of a slider was obtained by solving a modified Reynolds equation with finite volume method. The resulted forces and moments were fitted to form the performance functions and surfaces. A commercial slider design was illustrated.
4. An efficient scheme was enabled by combining the performance functions with the simplified suspension model. An unloading simulation was performance in a very short computational time. The effects of the suspension stiffnesses were studied.

References

- [1] M. SUK AND T. R. ALBRECHT, *The evolution of L/UL technology*, *Microsyst. Technol.*, 8 (2002), pp. 10–16.
- [2] D. B. BOGY, W. FONG AND B. H. THORNTON, *Some tribology and mechanics issues for 100Gb/in² hard disk drive*, *IEEE T. Magn.*, 38(5) (2002), pp. 1879–1885.
- [3] T. YAMADA AND D. B. BOGY, *Load-unload slider dynamics in magnetic disk drives*, *IEEE T. Magn.*, 24(6) (1988), pp. 2742–2744.
- [4] Q. H. ZENG, M. CHAPIN AND D. B. BOGY, *Dynamics of the unload process for negative pressure sliders*, *IEEE T. Magn.*, 35(2) (1999), pp. 916–920.
- [5] Q. H. ZENG AND D. B. BOGY, *A simplified 4-DOF suspension model for dynamic load unload simulation and its application*, *ASME J. Tribol.*, 122 (2000), pp. 274–279.
- [6] Y. LIU AND S. WANG, *A performance surface method for characterizing the nonlinear air bearing forces and moments with application to the unloading process*, *Proc. STLE/ASME Int. Joint Tribology Conf.*, (2008), Paper IJTC 2008-71193.
- [7] Y. LIU, H. J. DU AND S. WANG, *An efficient simulation scheme for the unloading process with application to parametric studies and trend analyses*, *Proc. JSME-IIP/ASME-ISPS Joint*

Conference on Micromechatronics for Information and Precision Equipment 2009, Paper 375027-3.

- [8] S. WANG, F. P. CRIMI AND R. J. BLANCO, *Dynamic behavior of magnetic head sliders and carbon wear in a ramp load process*, *Microsyst. Technol.*, 9 (2003), pp. 266–270.
- [9] W. HUA, B. LIU, G. SHENG AND J. LI, *Further studies of unload process with a 9D model*, *IEEE T. Magn.*, 37(4) (2001), pp. 1855–1858.
- [10] Y. HU, P. M. JONES AND K. LI, *Air bearing dynamics of sub-ambient pressure sliders during dynamic unload*, *ASME/STLE, International Tribology Conference*, 1998.
- [11] L. WU AND D. B. BOGY, *A generalized compressible Reynolds lubrication equation with bounded contact pressure*, *Phys. Fluid*, 13(8) (2001), pp. 2237–2244.
- [12] H. TANAKA, H. KOHIRA AND M. MATSUMOTO, *Effect of air-bearing design on slider dynamics during unloading process*, *IEEE T. Magn.*, 37(4) (2001), pp. 1818–1820.
- [13] A. BURGDORFER, *The influence of the molecular mean free path on the performance of hydrodynamic gas lubricated bearings*, *J. Basic Eng-T. ASME*, 81 (1959), pp. 94–100.
- [14] T. HSIA AND G. A. DOMOTO, *An experimental investigation of molecular rarefaction effects in gas lubricated bearings at ultra-low clearances*, *J. Lubric. Tech-T. ASME*, 105 (1983), pp. 120–130.
- [15] G. MITSUYA, *Modified Reynolds equation for ultra-thin film gas lubrication using 1.5-order slip-flow model and considering surface accommodation coefficient*, *J. Tribol-T. ASME*, 115 (1993), pp. 289–294.
- [16] R. F. GAN, *Lubrication theory at arbitrary Knudsen number*, *J. Tribol-T. ASME*, 107 (1985), pp. 431–433.
- [17] L. WU AND D. B. BOGY, *Use of an upwind finite volume method to solve the air bearing problem of HDDs*, *Comput. Mech.*, 26 (2000), pp. 592–600.
- [18] H. K. VERSTEEG, *An Introduction to Computational Fluid Dynamics: The Finite Volume Method*, Pearson Education, 2007.